Depth sensing indentation of organic–inorganic hybrid coatings deposited onto a polymeric substrate

L.A. Fasce, R. Seltzer, P.M. Frontini

PII: S0257-8972(12)00851-1
DOI: doi: 10.1016/j.surfcoat.2012.08.064
Reference: SCT 17959

To appear in: *Surface & Coatings Technology*

Received date: 28 May 2012
Accepted date: 28 August 2012

Please cite this article as: L.A. Fasce, R. Seltzer, P.M. Frontini, Depth sensing indentation of organic–inorganic hybrid coatings deposited onto a polymeric substrate, *Surface & Coatings Technology* (2012), doi: 10.1016/j.surfcoat.2012.08.064

DEPTH SENSING INDENTATION OF ORGANIC-INORGANIC HYBRID COATINGS DEPOSITED ONTO A POLYMERIC SUBSTRATE

L. A. FASCE[a] , R. SELTZER[b] AND P.M. FRONTINI[a]

[a] *INTEMA, National University of Mar del Plata-CONICET, Av. J. B. Justo 4302 (B7608FDQ), Mar del Plata, Argentina.*

[b] *IMDEA Materials Institute, C/Profesor Aranguren s/n, 28040 Madrid, Spain.*

lfasce@fi.mdp.edu.ar

rocio.seltzer@imdea.org

pmfronti@fi.mdp.edu.ar

Corresponding author: L. A. Fasce

Tel: +54-223-4816600 (int 183)

FAX: +54-223-4810046

ABSTRACT

PEO-Si/SiO_2 hybrid coatings deposited onto a PVC substrate were micromechanically characterized using depth sensing indentation. The effect of curing time and coating thickness were investigated. Elastic moduli of coated systems determined by the Oliver-Pharr approach displayed a continuous decreasing trend with increasing indentation depth, reflecting that the hybrids are stiffer than the substrate. Aiming to extract coating-only elastic modulus a simple method based on FE simulations was developed. The method was applied to evaluate the moduli of the hybrid coatings and the values were compared with those obtained by applying different approaches available in literature. The elastic modulus of PEO-Si/SiO_2 hybrids was proven to be practically independent of curing time after 24 hs. However, large curing times resulted in coatings being more prone to failure.

KEYWORDS

Depth sensing indentation, organic-inorganic hybrid coating, elastic modulus, numerical simulation.

1. INTRODUCTION

Organic-inorganic hybrids are widely used as polymeric protective coatings in optical, packaging, biomedical, microelectronics and decorative applications. Thanks to their ability to modify the mechanical and functional behavior of polymeric surfaces, they can enhance the surface performance of many polymers. For example, thin hybrids films are capable of improving the scratch resistance of transparent polymers such as poly(methyl methacrylate) (PMMA) and polycarbonate (PC) [1-5] and the wear resistance of polyester based resins, polyethylene (PE) and bisphenol-A polycarbonate (bis-A PC) [6-9]. Furthermore, hybrids can improve the barrier and antibacterial properties of polymer-based packaging materials like poly(vinyl chloride) (PVC) and PE [10,11]; and the oxygen barrier properties and water resistance of multilayered membranes based on poplypropylene (PP), low density polyethylene (LDPE) and poly(ethylene terephtalate) (PET) [12]. They can also enhance the flame resistance and thermal stability of PMMA, PET and LDPE [13,14]; and the photodegradation and yellowing resistance of PC [15]. In all cases, coating performance is controlled by the chemical composition of the hybrid as well as by its synthesis procedure [2,9,17-19]. In service conditions, these coating/substrate systems are subjected to different forms of loading, being their functionality and durability dependent on their mechanical performance, that is, the mechanical properties of the thin hybrid coating itself and the adhesion characteristics between coating and polymeric substrate.

This particular work faces the problem of the nanomechanical characterization of poly (ethylene oxide)/silica hybrid coatings (PEO-Si/SiO_2) deposited onto a flexible PVC substrate. Although, plasticized PVC is widely used in the production of a number of intra-corporeal medical devices, the migration of relatively low molecular weight additives may lead to adverse health effects in humans [20]. M. Messori and co-workers [19] proved that

PEO-Si/SiO_2 hybrid films can act as an efficient barrier coatings preventing plasticizer leaching from PVC. They also found that the barrier properties strongly depend on the organic/inorganic ratio as well as on the extent of reaction (curing time). A deep mechanical characterization of PEO-Si/SiO_2 hybrid films deposited onto PVC would contribute to optimize both coating formulation and processing conditions.

Depth sensing indentation, also called nanoindentation, appears as the most sound technique to characterize the mechanical behavior of thin hybrid coatings deposited onto substrates [21-24]. From indentation load-depth curves valuable mechanical quantities of hybrid coating/substrate systems such as elastic and plastic properties [1,16,17,25-28], creep properties [16], residual stresses [25,27], coating fracture toughness and adhesion interfacial fracture toughness (adhesion energy) [25,27,29-31] can be extracted.

The Oliver-Pharr approach is the most spread procedure of analysis used to determine elastic modulus and hardness [32] from indentation experiments. Although, originally developed for homogeneous materials, it has also been applied to determine properties of hybrid coating/substrate systems [17,27,33]. In some cases, the influence of the substrate in the indentation response makes the modulus values depend on penetration depth [17,34,35]. In such cases, the problem of determining coating–only properties is a difficult task due to the complex deformation process developed beneath the indenter. The coating response is influenced by several factors such as indenter geometry, coating and substrate mechanical properties, interfacial strength and coating thickness [17, 36-39].

Finite element (FE) analysis has been successfully used to interpret the indentation response of specific coating/substrate systems, typically metals [40-44]. In general, the approach is that of an inverse problem where the mechanical properties of the coating/substrate system are used as input to obtain the indentation load-displacement response and the stress field distribution beneath the indenter. Parametric studies are usually performed to understand the influence of tip geometry, coating thickness, and coating and

substrate mechanical properties on the indentation response of the coating/substrate system.

In this work, measured and simulated indentation experiments are combined to mechanically characterize four PEO-Si/SiO_2 hybrid coatings deposited onto PVC. The studied systems differ in coating thickness and curing time. The deformation characteristics of real systems are first investigated using imaging techniques and then the elastic moduli are obtained by the Oliver-Pharr approach as a function of indentation depth. FE indentation simulations are performed to give insight into the deformation behavior that leads to coating failure and to analyze the influence of properties mismatch on the apparent elastic modulus of the system. An inverse problem approach based on FE simulation is used to develop an algorithm to determine the intrinsic moduli of PEO-Si/SiO_2 hybrids. The values are compared with those obtained by applying different approaches available in literature.

2. EXPERIMENTAL

2.1. MATERIALS

Four samples of a commercial PVC film (150μm in thickness) coated with PEO-Si/SiO_2 based hybrids differing in coating thickness and curing time are characterized (Table I). The actual coating thickness values given in Table I were determined by Scanning Electron Microscopy (SEM) using a JEOL JSM-6460LV microscope. The samples were cryofractured and coated with a thin film of Au/Pd before inspection. A typical SEM micrograph is shown in Figure 1.

This type of hybrids has a nanocomposite structure with a high level of interpenetration between organic (PEO) and silica (inorganic) phases [19].

2.2 DEPTH SENSING INDENTATION EXPERIMENTS

Depth sensing indentation technique was used to characterize the PEO-Si/SiO_2//PVC

systems. Tests were performed in a Triboindenter (Hystitron Inc.) at room temperature. Experiments involved complete loading-holding-unloading cycles under load controlled conditions (trapezoidal loading functions) with the continuous measurement of applied load and displacement (tip penetration depth). Thermal drift correction was applied to displacement data following the Hysitron recommended procedure. Maximum loads ranging from 70 to 2500μN were applied using a Berkovich tip and a loading/unloading rate of 50μN/s. A holding time of 15s was applied at maximum load before unloading to minimize viscoelastic effects in the unloading curve [45,46].

2.3 DETERMINATION OF MECHANICAL PROPERTIES

The indentation elastic modulus was determined as a function of indentation depth from the load–depth (*P*-*h*) curves using the approach outlined by Oliver and Pharr [32]. This method is based on the assumption that the material behavior during unloading is purely elastic, and it is described as follows:

The unloading part of the *P*-*h* curve is fitted through a power law function:

$$P = A(h - h_f)^m \tag{1}$$

and the contact stiffness (*S*) is calculated from slope of unloading curve as:

$$S = \left.\frac{dP}{dh}\right|_{h_{\max}} = mA(h_{\max} - h_f)^{m-1} \tag{2}$$

being *A* and *m* the power law function fitting parameters, h_f the residual penetration depth and $h_{\max}$ the maximum penetration depth achieved after the holding period. The contact depth h_c is calculated by:

$$h_c = h_{\max} - \varepsilon \frac{P_{\max}}{S} \tag{3}$$

where ε a tip geometry factor, usually taken as 0.75. The reduced elastic modulus (E_r) was then calculated as:

$$E_r = \frac{S\sqrt{\pi}}{2\sqrt{A_c}} \tag{4}$$

where A_c is the actual contact area which accounts for the non-ideal shape of the tip. A_c was fitted to a polynomial function of h_c using a series of indentations performed on a fused quartz standard. E_r is directly related to the Young's modulus of the sample, E, by:

$$E_r = \left[\frac{1-\nu^2}{E} + \frac{1-\nu_i^2}{E_i}\right]^{-1} \tag{5}$$

where E_i and ν_i are the Young's modulus and the Poisson´s ratio of the indenter (1140GPa and 0.07) while E and ν are the sample properties.

Furthermore, the yield stress (σ_y) of PVC was estimated by the inverse method proposed by Dao et al. [47].

2.4 FINITE ELEMENT SIMULATIONS

Simulated indentations were carried out using a finite element (FE) commercial software ABAQUS 6.11 (2011). Coating/substrate fictitious systems were modeled as bodies of revolution. Axisymmetric linear quadrilateral elements were adopted, where a fine mesh (2000 elements concentrated towards the indenter tip) was used close to the contact zone (its size was a rectangle of 1 μm in length and the coating thickness in height) to capture the stress concentration and its gradient under the indenter, and a coarse mesh (5500 elements) outside this region to economize computation time. An equivalent conical tip with apical angle of 19.7º was used to simulate the Berkovich pyramid shaped indenter since it gives the same area function. The indenter was assumed infinitely rigid because the elastic modulus of the tip material used in physical experiments is several orders of magnitude higher than the elastic modulus of the coating/substrate systems (diamond, E=1140GPa). Frictionless contact was defined between the surface of the indenter and that of the specimen.

The substrate material was modeled as isotropic elastic-perfectly-plastic Von Mises

solid and the coating behavior was assumed purely elastic. The values of the elastic modulus, Poisson's ratio and yield stress used in the simulations are detailed in Table II. The properties of the PVC were determined from the physical nanoindentations results as explained in section 2.3. The elastic moduli of the coating are hypothetical but within a realistic range [16]. Constant Poisson's ratios were used for both coating and substrate since the effect of Poisson ratio on indentation behavior is very small [48].

The coating and substrate were assumed perfectly bonded. This is because, in the real systems excellent adhesion is expected due to the presence of ether linkages in PEO that lead to intermolecular association complexes with PVC due to the strong hydrogen bonding character of the ether oxygens [19].

3. RESULTS AND DISCUSSION

3.1 INDENTATION LOAD-DEPTH CURVES AND COATING DAMAGE

Typical indentation curves measured for the coating/substrate systems under different maximum applied loads are shown in Figures 2-*a* and *b*. For comparison, the substrate response alone is also included. It is evident that the micromechanical response of the PVC surface changes markedly with the presence of the PEO-Si/SiO_2 coating.

The uncoated PVC substrate deforms plastically and shows a large amount of creep during the holding stage at maximum load. The substrate response is highly repetitive as demonstrated by the superimposed loading curves obtained at increasing maximum applied forces (Fig. 2-*a*).

The indentation response of the coating/substrate systems display different characteristics, which vary with increasing applied maximum load. At relatively low loads (Fig. 2-*a*), the response is characterized by a lower penetration depth at any given load, decreased plastic work of indentation (denoted by the area enclosed within the loading-

unloading curves), increased amount of elastic recovery in the indenter displacement during unloading, and negligible creep, compared to the uncoated PVC. Smooth variations in the unloading curves are observed as the indenter penetrated deeper into the sample. The response changed drastically when the indenter reached a certain depth denoted by a marked discontinuity in the loading curve (Fig. 2-*b*). Once the load discontinuity appears, the loading curve tends to resemble the substrate response upon further increasing the load. The critical point, defined either by the depth to coating thickness ratio values (h_{cr}/t) or its corresponding load (P_{cr}) at which discontinuities appeared, are reported in Table III for all the coated systems. These critical values indicate that the failure of the hybrid coating occurs well before the Berkovich tip reaches the coating/substrate interface. Note that there is not a clear trend in P_{cr} values but evidently h_{cr}/t decreased with increasing curing time.

This type of discontinuities in load-depth curves are usually attributed to coating failure events occurring in response to indentation stresses in hard coating/soft substrate systems [22,31,49]. Typically coating chipping off leads to a significant change in the load-depth curve shape since considerable displacement at constant load takes place [50].

A SEM image showing the typical impression left on the coating surface after the application of an indentation cycle with a maximum load higher than P_{cr} is shown in Figure 3. SEM inspection evidences coating failure and explains the shape change in the curves at loads higher than P_{cr}. It is evident that circumferential cracking and finally coating chipping off occurred. Then, the indenter continued penetrating into the PVC substrate leaving on the surface a pyramidal shaped impression.

It has been stated that for a hard coating/soft substrate system, the substrate yields first with the coating being elastically deform [22]. A variety of cracking events like edge cracks parallel to the free surface, circumferential cracks, bending cracks at the coating/substrate interface, and inclined cracks through the film thickness may occur depending on coating thickness, properties mismatch, indenter geometry and load [40]. All these events are forced

by an incompatibility in displacements due to substrate plastic deformation. The coating fractures because it is unable to accommodate substrate plasticity.

To study the influence of the coating/substrate elastic modulus mismatch (E_c/E_s) on the indentation response, finite element simulations of indentation tests were performed. Two extreme cases were simulated, namely, a system with an elastic mismatch E_c/E_s=1.8 and another one with E_c/E_s=25. The relative indentation depth (h/t) was equal to 0.1. Figure 4 gives the Von Mises and maximum stress fields and the plastic zone extension.

The location of the superficial circumferential cracks in Figure 3 coincides with the location of the highest normal stresses around the contact region (Fig. 4-*a*). Another site of stress concentration in the coating is located beneath the indenter at the coating/substrate interface (Fig. 4-*b*), which seems to be responsible for the final coating chipping off [i.e. 51,52]. Indeed, a large plastic zone is developed in the substrate beneath the indenter at low indentation depths (Fig. 4-*c*), well before the coating fails.

By comparing the results for the different simulated coating/substrate systems it is observed that the greater the mismatch between the mechanical properties of the coating and substrate, the greater the stresses generated in the coating, which in turn, promotes failure. The stresses generated in the substrate are compressive in the case of the stiffest coating, while they are compressive and tensile in the case of the most compliant coating. This is due to more spread load distribution exerted by the rigid layer compared to the more compliant one. The substrate experienced plastic deformation in the case of the stiffer coating, but it remained in the elastic regime in the case of the more compliant coating. This occurs because the compliant coating absorbs a larger part of the imposed deformation (or displacement) compared to the stiffer coating.

Then, it is concluded that a stiffer coating is more prone to fracture than a more compliant one (having both of them the same yield strength) under the same applied displacement.

3.2 DETERMINATION OF THE COATINGS ELASTIC MODULI

For each PEO-Si/SiO_2// PVC system, the Oliver-Pharr analysis is used to determine the elastic modulus as a function of indentation depth. Only the curves for which the maximum penetration depth is lower than that of the critical point (values already reported in Table III) are considered. This is done to avoid underestimation of elastic modulus caused by coating failure events [24].

The results are shown in Figure 5. For all PEO-Si/SiO_2// PVC systems, elastic modulus values exhibit a monotonic decrease with indentation depth in the whole range measured. The determined values represent an apparent modulus, E_a, which combines the mechanical properties of coating and substrate. It has to be pointed out that E_a values does not exhibit a plateau value at indentation depths lower than 10% of coating thickness. Thus, the "10% rule" commonly used to evaluate the intrinsic modulus of coatings [1,22,25,32] is not applicable to our systems.

To extract the intrinsic elastic modulus of the hybrid coatings, E_c, from apparent values (E_a), a method based on our FE simulation results was developed and it is presented in section 3.3.1. Other approaches available in literature are considered in section 3.3.2. All methodologies are applied to the four PEO-Si/SiO_2//PVC systems.

3.2.1 A method based on FE simulations

In this section, a suitable procedure to single out the elastic modulus of a stiff coating deposited on a soft substrate is proposed. To this aim, the indentation *P*-*h* curves for different coating/substrate systems listed in Table II were simulated and the E_a values calculated. Results for the different parameter combinations are shown in Figure 6. It can be seen that independently of the coating/substrate compliance mismatch, E_a monotonically tends to the coating modulus towards zero depth. The non-linearity between E_a and *h/t* is accentuated by

increasing coating/substrate compliance mismatch.

The proposed method consists of an equation that relates the apparent elastic modulus E_a determined at a fixed relative indentation depth $(h/t)^*$ and the known elastic modulus of the substrate E_s with the elastic modulus of the coating E_c. In principle, $(h/t)^*$ is chosen to be lower than the critical coating failure values (see Table III). Furthermore, other factors such as the influence of substrate plasticity and the estimation of the contact area by the Oliver-Pharr method are considered, as described in the following.

A comparison of the apparent values emerging from elastic coating onto elastic substrate and elastic coating onto elasto-plastic substrate is shown in Figure 7. This plot shows that the apparent elastic modulus is lowered by substrate plasticity. The influence depends on compliance mismatch: the stiffer the coating, the less the influence of substrate plastic flow on apparent modulus. It can be seen in Figure 7 that for h/t = 0.1 the substrate plastic flow does not markedly affect the decay in apparent modulus due to compliance mismatch.

In the Oliver-Pharr approach, the reduced elastic modulus is inversely proportional to the square root of the contact area (Eq. 4), which in turn depends on the contact depth that is estimated from the contact stiffness (Eq. 3). In this analysis there is always some downward elastic deformation of the material surface and it is known that hard film on soft substrate systems tend to sink-in when indented (see for example in [34]). The values of the projected contact area data arisen from Oliver-Pharr analysis of simulated load-depth curves are compared with the contact area values at maximum load of FE simulations (Fig. 8). The latter are obtained from the contact radius values, a, directly checking the contact status of the nodes on the sample surface under maximum load and using the relationship $A_c=\pi a^2$ for the equivalent conical indenter. As shown in Figure 8 for indentations performed at h/t equal to 0.1, no striking differences between both contact area values are found for E_c values lower than 20GPa. As well, stiffer coatings only a small error (lower than 10%) is observed. For

very stiff coatings, a slightly larger sinking-in effect than that considered in the Oliver-Pharr approach appears to occur at the surface.

The apparent modulus value at $(h/t)^*$=0.1 is finally adopted to perform the correlation between E_a and E_c values. Figure 9 shows the correlation found between the dimensionless parameters E_c/E_s and E_a/E_s. These simulated data were accurately fitted using a second order polynomial function, as judge by the obtained minimum squares regression coefficient (R= 0,99997). The correlation is given by:

$$\frac{E_c}{E_s} = 0.1679\left(\frac{E_a}{E_s}\right)^2 + 0.98\frac{E_a}{E_s} - 0.2058 \quad (6)$$

This simple equation allows determining the intrinsic elastic modulus of the coating E_c if the following parameters are known:

- the coating thickness, t
- the apparent elastic modulus of the coating/substrate system determined by the Oliver-Pharr approach from a nanoindentation tests performed at $(h/t)^*$=0.1using a sharp Berkovich tip.
- the substrate modulus, E_s

Eq. 6 is applicable to coating/substrate systems that comply with the following characteristics:

- $E_s/\sigma_{ys} < 70$
- $1.8 < E_c/E_s < 25$
- the coating is homogeneous, isotropic, its thickness is uniform
- the coating has good adhesion with the substrate in such a way that no discontinuities are detectable in the experimental loading curve up to $(h/t)^*$=0.1.

The elastic moduli of the PEO-Si/SiO_2 hybrids obtained through this method are given in Table 4. To verify the accuracy of the method, the obtained E_c were used as inputs in FE simulations. The indenter geometry was modeled considering the actual contact area of the Berkovich tip used in this study (a polynomial function of h_c determined from physical

nanoindentations performed on a standard fused-quartz sample). The simulated load-depth data are analyzed to predict apparent modulus values as a function of penetration depth. The results are shown in Figures 10 and 11. The proposed method appears to be very accurate as demonstrated by the superposition of both simulated and measured *P*-*h* curves (Fig. 10). Furthermore, the physically measured trend of apparent elastic modulus presents a close correlation with the predicted one (Fig. 11). The proposed method seems to work reasonably well despite the differences between the real and idealized tip shape and the mechanical behavior of coating and substrate. Moreover, it can be concluded that the PEO-Si/SiO_2 coatings are mechanically homogeneous.

According to the obtained values, the elastic modulus of the PEO-Si/SiO_2 hybrids is slightly increased by curing times larger than 24 hs (Table IV).

The stress distribution beneath the indenter at which the actual PEO-Si/SIO_2 // PVC systems failed (Table III) is quantified using FE simulations taken into account the determined coating moduli. The coating is assumed to be perfectly bonded to the substrate and the formation of edge cracks is neglected. The maximum normal stress values achieved at coating-substrate interface are reported in Table V and a typical maximum normal stress contour is shown in Figure 12. The maximum normal stress decreases with increasing curing time and it is affected by coating thickness. This simplified analysis suggests that there is a detriment in interfacial strength between PEO-Si/SiO_2 hybrids and PVC when increasing curing time. These results are in agreement with the worsening of the anti-leaching properties observed by M. Messori et al. [19] due to a weakening of the interfacial strength. As well, a large plastic zone is confirmed to develop in the PVC substrate.

3.2.2 Fitting/extrapolation based methods and weight function models

Elastic moduli values obtained in the previous section are here compared with the ones arisen from other approaches available in literature, in which no numerical simulations are

needed.

The simplest method to evaluate the intrinsic elastic modulus of a coating is by fitting the E_a vs. h_c/t (or a/t) data with an arbitrary mathematical function and then extrapolating the E_a value to zero depth. ISO 14577-4:2007 Standard, suggests a linear relationship considering only data within a/t <2 [53]. Other mathematical functions like Gaussean, exponential and polynomial are also usually adopted (see for example in [17,35]). E_c values arising from the fitting of all available experimental data using either Linear (ISO 14577-4:2007), Gaussean and second order polynomial functions are listed in Table IV. In the case of ISO 14577-4:2007 method, the experimental thickness normalized contact depth range was lower than the required one because of coating failure. In order to meet the required range, a blunt indenter should be used. E_c values obtained by zero-depth extrapolating methods are lower than the ones thrown by the FEA method. The Gaussean type function is the best at describing the experimental data as judged by the regression coefficient value. However, the extrapolated E_c values depend on the fitting range. For each material data set, E_c decreases if the lower limit of h_c/t range is shifted to larger values. The accuracy of this procedure could be improved taking into account data of very shallow indentations (h/t about 0.01) as demonstrated for hybrid coatings onto PC substrate by Soloukhin [17]. In their work, the fitting/extrapolation method appears to work reasonably well because coatings are relatively thick (around 20-100μm). However, *P-h* data at penetration depths lower than 20nm are difficult to perform and analyze without inducing important errors due to thermal drift, surface roughness and tip area calibration.

Another way to determine the coating–only elastic modulus of thin films is to represent the apparent property as a combination of coating and substrate moduli or compliances in relation to the contact indentation depth, the coating thickness and various parameters, using a weight function, ϕ. Typically, exponential weight functions have been proposed (see for example the review presented in [44]). Equations based on weight functions

expressed in terms of *t/h* predict a plateau modulus for low depth values. Among them there is the model developed by Doerner and Nix [54] and the one proposed by Antunes et. al [44]. On the other hand, equations expressed in terms of *h/t* yield a continuous decrease of the apparent property from that of the coating to that of the substrate, like the direct (MD) and reciprocal (MR) models proposed by Mencík et al. [55] and the semi-empirical Gao model [56]. In the latter, the weight function, ϕ, is a complex function of the contact radius at maximum applied load, *a*, which is based on the analytical solution of the contact of a rigid cylindrical indenter with an elastic layered body [55]. Even if it was originally obtained for a cylindrical flat punch indentation, it is assumed to be equivalent to a conical indentation having half-angle ψ of 70.32º (Berkovich tip), as follows: $a = h_c \tan\psi$ [38].

Since PEO-Si/SiO_2 // PVC systems do not display a plateau value at low depths (Fig. 5), only models in which the weight functions are expressed in terms of *h/t* are selected to fit the experimental data. The equations for each model are given in Table IV. In the fitting procedures, E_s and *t* are taken as known parameters. For MD and MR models [55], equations are developed in linear forms and model parameters (E_c and α_{MD} or E_c and α_{MR}) are obtained using minimum least squares. For the Gao et al. model, the equation is transformed to a straight line that crosses the origin of the coordinate systems ($y=Ax$), the constant *A* calculated using a least squares method and the elastic modulus of the coating alone obtained by $E_c = E_s+A$. The results are shown in Table IV. Both MD and MR models adequately describe the E_a *vs* h_c/t experimental trend while the Gao model displays a bad correlation. The E_c values obtained from MD and MR models are close to the ones obtained by FEA method. The main advantage of MD and MR models is that they can be applied to cases in which the thickness of the coating is unknown.

4. CONCLUSIONS

Four PEO-Si/SiO_2//PVC systems differing in coating thickness and reticulation time

were mechanically characterized by depth sensing indentation. Coating/substrate systems and substrate alone displayed very different indentation behaviors. PVC did exhibit plastic deformation while coated samples behave in a more elastic way. Indentation curves exhibited discontinuities consistent to the appearance of coating failure events.

Elastic moduli of PEO-Si/SiO_2//PVC systems determined by the Oliver-Pharr approach displayed a continuous decreasing trend with increasing indentation depth. To give insight into this complex issue, experiments were complemented with numerical simulations performed on fictitious systems composed by elastic films of different modulus perfectly bonded to an elastoplastic substrate.

FE simulations demonstrated that the elastic modulus of coating/substrate systems (apparent modulus) depends on the compliance mismatch between coating and substrate but also on the substrate plasticity. The plastic deformation of the substrate causes an extra reduction in apparent modulus with respect to the drop due to the elastic mismatch. The stiffer the coating the less is the influence of substrate plastic flow on apparent modulus.

With the aid of FE simulations the intrinsic elastic modulus of PEO-Si/SiO_2 coatings could be successfully extracted from the apparent values determined by the Oliver-Pharr approach taking into account the effects of coating/substrate elastic mismatch and substrate plasticity. PEO-Si/SIO_2 hybrids behave as homogeneous materials. So, the decreasing trend in the apparent modulus with indentation depths is due to difference in mechanical properties of coating and substrate and not due to a gradient of modulus in the hybrid film. The curing time has a slight effect on elastic modulus of PEO-Si/SIO_2 hybrids.

Additionally, several approaches which avoid the need of using numerical simulations were tried to extract the intrinsic coating's elastic modulus. Unfortunately, the Gao et al. model [56], a second order polynomial, a Gaussian type mathematical function and the linear trend proposed in ISO 14577-4 failed in describing the trend of apparent elastic modulus displayed by PEO-Si/SIO_2//PVC systems. Conversely, it could be well described using the

simple approaches proposed by Mencík et al. (MD and MR) [55]. Moreover, the fitted elastic modulus values were close to the ones obtained by our FE based method. The MD and MR equations could be useful to analyze systems in which coating thickness is unknown and FE simulations cannot be performed.

PVC substrate plasticity played a central role in coating's failure promoting bending stresses that induced coating cracking and finally chipping off. The increase in reticulation time seems to induce a detriment in the interfacial strength of PEO-Si/SiO_2 //PVC systems as it emerged from the experimental h_{cr}/t values and the simulated maximum normal stress developed at interface. On the other hand, interfacial strength appeared to be unaffected by coating thickness.

5. AKNOWLDEGMENTS

Authors would like to express their grateful to Dr. Paola Fabbri from University of Módena and Dr. Claudia Marano from Politecnico di Milano for kindly supplying the PEO-Si/SiO_2//PVC systems used in this research. L. Fasce also thanks to CONICET for the financial support (PICT 01160). R Seltzer acknowledges the support from the Spanish Ministry of Science and Innovation through the Juan de la Cierva program.

6. REFERENCES

[1] D. Blanc, A. Last, J. Fanc, S. Pavan, J-L. Loubet, Thin Solid Films 515 (2006) 942-946.

[2] P. Fabrri, B. Singh, Y. Leterrier, J.A.E. Manson, M. Messori, F. Pilati, Surf. Coat. Technol. 200 (2006) 6706-6712.

[3] P. Fabbri, M. Messori, M. Toselli, P. Veronesi, J. Rocha, F. Pilati, Adv. Polym. Tech. 27 (2009) 117-126.

[4] L.Y.L. Wu, E. Chwa, Z. Chen, X.T. Zeng, Thin Solid Films 516 (2008) 1056–1062.

[5] W. Shen, B. Jiang, S.M. Gasworth, H. Mukamal, Tribol. Int. 34 (2001) 135-142.

[6] T. P. Chou, G. Cao, J. Sol-Gel Sci. Technol. 27 (2003) 31-41.

[7] Y.-H. Han, A. Taylor, K. M. Knowles, Surf. Coat. Technol. 203 (2009) 2871-2877.

[8] M. Toselli, P. Marini, P. Fabbri, M. Messori, F. Pilati, J. Sol-Gel Sci. Technol. 43 (2007) 73-83.

[9] C. Li, K. Jordens, G.L. Wilkes, Wear 242 (2000) 152–159.

[10] R. Iseppi, F. Pilati, M. Marini, M. Toselli, S. de Niederhäusern, E. Guerrieri, P. Messi, C. Sabia, G. Manicardi, I. Anacarso, M. Bondi, Int. J. Food Microbiol. 123 (2008) 281-287.

[11] M. Marini, S. De Niederhausern, R. Iseppi, M. Bondi, C. Sabia, M. Toselli, and F. Pilati, Biomacromolecules 8 (2007) 1246-1254.

[12] M. Minelli, M. G. De Angelis, F. Doghieri, M. Rocchetti, A. Montenero, Polym. Eng. Sci. 50 (2010) 144–153.

[13] M. Messori, M. Toselli, F. Pilati, E. Fabbri, P. Fabbri, S. Busoli, L. Pasquali, S. Nannarone, Polymer 44 (2003) 4463–4470.

[14] M. Marini, F. Pilati, A. Saccani, and M. Toselli, Polym. Degrad. Stab. 93 (2008) 1170-1175.

[15] P. Fabbri, C. Leonelli, M. Messori,F. Pilati,M. Toselli, P. Veronesi, S. Morlat-Thérias, A. Rivaton, J. L. Gardette, J. Appl. Polym. Sci. 108 (2008) 1426–1436.

[16] A.J. Atanacio, B.A. Latella, C.J. Barbe, M.V. Swain, Surf. Coat. Technol. 192 (2005) 354-364.

[17] V.A. Soloukhin, W. Posthumus, J.C.M. Brokken-Zijp, J. Loos, G. de With, Polymer 43 (2002) 6169–6181

[18] C. Marano, F. Briatico-Vangosa, M. Marini, F. Pilati, M. Toselli, Eur. Polym. J. 45 (2009) 870–878.

[19] M. Messori, M. Toselli, F. Pilati, E.Fabbri, P. Fabbri, L. Pasquali, S. Nannarone, Polymer 45 (2004) 805-813.

[20] J.A. Tickner, T. Schettler, T. Guidotti, M. McCally, M. Rossi, Am J Ind Med 39 (2001) 100-111.

[21] F. Mammeri, E. Le Bourhis, I. Rozes, C. Sanchez, J. Mater. Chem 15 (2005) 3787-3811.

[22] J. Bull, J. Phys. D: Appl. Phys. 38 (2005) R393-413.

[23] B. Bhushan, X. Li, nt. Mater. Rev. 48 (2003) 125-164.

[24] J. Malzbender, J.M. J. den Tooner, A.R. Balkenende, G. de With, Mater. Sci. Eng., R 36 (2002) 47-103.

[25] S. Etienne-Calas, A. Duri, P. Etienne, J. Non-Cryst. Solids 344 (2004) 60-65.

[26] J.H. Yim, Y. Lyu, H.D. Jeong, S.K. Mah, J. Hyeon-Lee, J.H. Hahn, G.S. Kim, S. Chang, J.G. Park, J Appl. Polym. Sci. 90 (2003) 626-634.

[27] A. Ferchini, S. Calas-Etienne, M. Smaihi, P. Etienne, J. Non-Cryst. Solids 354 (2007) 712-716.

[28] Z.L. Li, J.C.M. Brokken-Zijp, G. de With, Polymer 45 (2004) 5403-5406.

[29] J. den Toonder, J. Malzbender, G. de With, R. Balkenende, J. Mater. Res. 17 (2002) 224-233.

[30] J. Malzbender, G. de With, Surf. Coat. Technol. 135 (2000) 60-68.

[31] J. Malzbender, G. de With, Surf. Coat. Technol. 137 (2001) 72-76.

[32] W.C. Oliver, G.M. Pharr, J. Mater. Res. 7 (1992) 1564-1583.

[33] M.A. Robertson, R.A. Rudkin, D. Parsonage, A. Atkinson, J. Sol-Gel Sci. Technol. 26 (2003) 291-295.

[34] R. Saha, W.D. Nix, Acta Mater. 50 (2002) 23-38.

[35] E. Le Bourhis, Vacuum 82 (2008) 1353-1359.

[36] A. A. Pelegri, X. Huang, Compos. Sci. Technol. 68 (2008) 147-155.

[37] N. Chollacoop, L- Li, A. Gouldstone, Mater. Sci. Eng., A 423 (2006) 36-40

[38] A. Tricoteaux, G. Duarte, D. Chicot, E. Le Bourhis, E. Bemporad, J. Lesage, Mech. Mater. 42 (2010) 166-174.

[39] J. Hay, B. Crawford, J. Mater. Res. 26 (2011) 727-738.

[40] S. Math, S. J. Suresha, V. Jayaram, S. K. Biswas, J. Mater. Sci 41 (2006) 7830-7837.

[41] S.K. Vanimisetti, R. Narasimhan, Int. J. Sol. Struct. 43 (2006) 6180-6193.

[42] T.Y. Tsui, J. Vlassak and W.D. Nix, J. Mater. Res. 14 (1999) 2204-2209.

[43] Z.-H. Xu, D. Rowcliffe, Thin Solid Films 447-448 (2004) 399-405.

[44] J.M. Antunes, J.V. Fernades, N.A. Sakharova, M.C. Oliveira, L.F. Menezes, Int. J. Sol. Struct. 44 (2007) 8313-8334.

[45] K.B. Geng, F.Q. Yang, T. Druffel, E.A. Grulke, Polymer 46 (2005) 11768-11772.

[46] A.H.W. Ngan, B. Tang, J. Mater. Res. 17 (2002) 2604-2610.

[47] M. Dao, N. Chollacoop, K.J. Van Vliet, T.A. Venkatesh, S. Suresh, Acta Mater 49 (2001) 3899–3918.

[48] Y.-T Cheng, C.-M. Cheng, Int. J. Solids Struct. 36 (1999) 1231-1243.

[49] R. Andresson, G. Toth, L. Gan, M.V. Swain, Eng. Fract. Mech. 61 (1998) 93-105.

[50] J. Malzbender, G. de With, Surf. Coat. Technol. 127 (2000), 265-272.

[51] M. Bartsch, H. Linder, I. Mircea, J. Suffner, B. Baufeld, Key Eng. Mat. 290 (2005) 183-190.

[52] J. Yan, T. Leist, M. Bartsch, A.M. Karlsson, Acta Mater. 56 (2008) 4080-4090.

[53] ISO 14577-4:2007(E) International Standard. Metallic materials-Instrumented indentation test for hardness and materials parameters- Part 4: Test method for metallic and non-metallic coatings.

[54] M.F. Doerner, W.D. Nix, J. Mater. Res. 1 (1986) 601-609.

[55] J. Mencík J., D. Munz, E. Quandt, E.R. Weppelmann, M.V. Swain, J. Mater. Res. 12 (1997) 2475-2484.

[56] H.J. Gao, C.H. Chiu, J. Lee, Int. J. Sold. Struc. 29 (1992) 2471-2492.

8. CAPTIONS TO FIGURES

Figure 1. SEM micrograph showing coating thickness determination for A3b system.

Figure 2. Load-depth curves obtained in physical indentation experiments for: **a)** A3b system - experiments at which coating failure conditions were not achieved; **b)** A1 system- the arrow indicates the appearance of coating failure events. The substrate-alone response is also included.

Figure 3. SEM micrograph of a typical indentation residual impression in A2 system for maximum indentation load larger than P_{cr} (1000μN).

Figure 4. Contours plots of: **a)** Von Mises equivalent stress; **b)** maximum normal stress; **c)**

plastic zone. The substrate is PVC (E_s=2.8GPa, σ_y=40MPa, v=0.4) coated with an elastic material of either 5 or 70GPa in modulus (v=0.4). Relative indentation depth is h/t=0.1.

Figure 5: Apparent elastic modulus as a function of contact depth to thickness ratio for the PEO-Si/SiO_2 // PVC systems. The dashed line represents the modulus determined for the uncoated PVC (2.8GPa).

Figure 6: Effective elastic modulus to coating modulus ratio versus thickness-normalized penetration depth for simulated elastic coatings onto elasto-plastic substrate *systems.*

Figure 7: Comparison of simulated apparent elastic modulus versus h/t for elastic coatings onto purely elastic and elasto-plastic substrate systems.

Figure 8: Comparison of contact area obtained from simulated contact radii and from contact depth arisen from *O&P* approach as a function of coating modulus for h/t=0.1.

Figure 9: Correlation between coating elastic modulus and apparent elastic modulus normalized by substrate modulus for h/t=0.1.

Figure 10: Comparison of physically measured and simulated nanoindentation load-depth curves for A1 system.

Figure 11: Apparent modulus values as a function of thickness normalized penetration depth for A3b system.

Figure 12: Maximum Normal Stress contour for simulated A3b system.

Table I. *Sample denomination, coating thickness and curing time of PEO-Si/SiO_2//PVC systems.*

Sample	A1	A2	A3	A3b
Coating thickness (μm)	0.41	0.37	0.61	1.42
Curing time (h)	24	50	168	168

Table II*. Materials properties used in FE simulations.*

	Elastic modulus (GPa)	Poisson's ratio	Yield Stress (MPa)
Substrate (PVC)	2.8	0.4	40
Coating	5,10, 20, 50, 70	0.4	∞

Table III. *Critical point at which discontinuities appeared in indentation loading curve for real systems.*

Sample	A1	A2	A3	A3b
h_{cr}/t	0.74 ± 0.06	0.52 ± 0.05	0.30 ± 0.02	0.28 ± 0.02
P_{cr} (μN)	715 ± 85	276 ± 42	346 ± 30	1813 ± 215

Table IV. *Intrinsic elastic moduli of PEO-Si/SiO_2 hybrids determined by FEA method and by other approaches described in section 3.2.2.*

Method / System	E_c [GPa] (R)			
	A1	**A2**	**A3**	**A3b**
FEA method	8.1	7.9	8.9	9.2
ISO 14577-4:2007 method [53]	7.6 (-0.93168)	6.8 (-0.90376)	7.1 (-0.98365)	7.8 (-0.97744)
Second order Polynomial fitting function	7.5 (0.86813)	7.2 (0.84738)	7.1 (0.96757)	8.1 (0.96022)
Gaussean fitting function	7.0 (0.96739)	7.3 (0.93794)	6.9 (0.96861)	7.7 (0.98473)
Mencick et. al (MD) [55] $\frac{\left\|E^*_{ap}-E^*_s\right\|}{\left\|E^*_c-E^*_s\right\|}=\exp\left(-\alpha_{DN}\frac{h_c}{t}\right)$	8.0 (0.93507)	7.0 (0.92321)	7.6 (0.97849)	8.3 (0.97718)
Mencick et al. (MR) [55] $\frac{\left\|\frac{1}{E^*_{ap}}-\frac{1}{E^*_s}\right\|}{\left\|\frac{1}{E^*_c}-\frac{1}{E^*_s}\right\|}=\exp\left(-\alpha_{MR}\frac{h_c}{t}\right)$	8.5 (0.93017)	7.2 (0.92561)	8.2 (0.97254)	8.8 (0.97357)
Gao et al. [56] $\frac{\left\|\frac{1}{E^*_{ap}}-\frac{1}{E^*_s}\right\|}{\left\|\frac{1}{E^*_c}-\frac{1}{E^*_s}\right\|}=\phi^{a}$	7.5 (0.83296)	7.1 (0.83235)	6.4 (0.72708)	6.7 (0.54447)

[a] $\phi=\frac{2}{\pi\arctan\left(\frac{t}{a}\right)}+\frac{1}{2\pi(1-\nu)}\left[(1-2\nu)\left(\frac{t}{a}\right)\ln\left(\frac{1+\left(\frac{t}{a}\right)^2}{\left(\frac{t}{a}\right)^2}\right)-\frac{\left(\frac{t}{a}\right)}{1+\left(\frac{t}{a}\right)^2}\right]$

Table V. *Relevant values arisen from simulation of stress and strain distribution at critical indentation point for real* PEO-Si/SIO_2 // PVC *systems.*

Sample	**A1**	**A2**	**A3**	**A3b**
Critical depth (μm)	0.303	0.192	0.183	0.398
Maximum normal stress at coating-substrate interface (GPa)	0.90	0.68	0.41	0.42

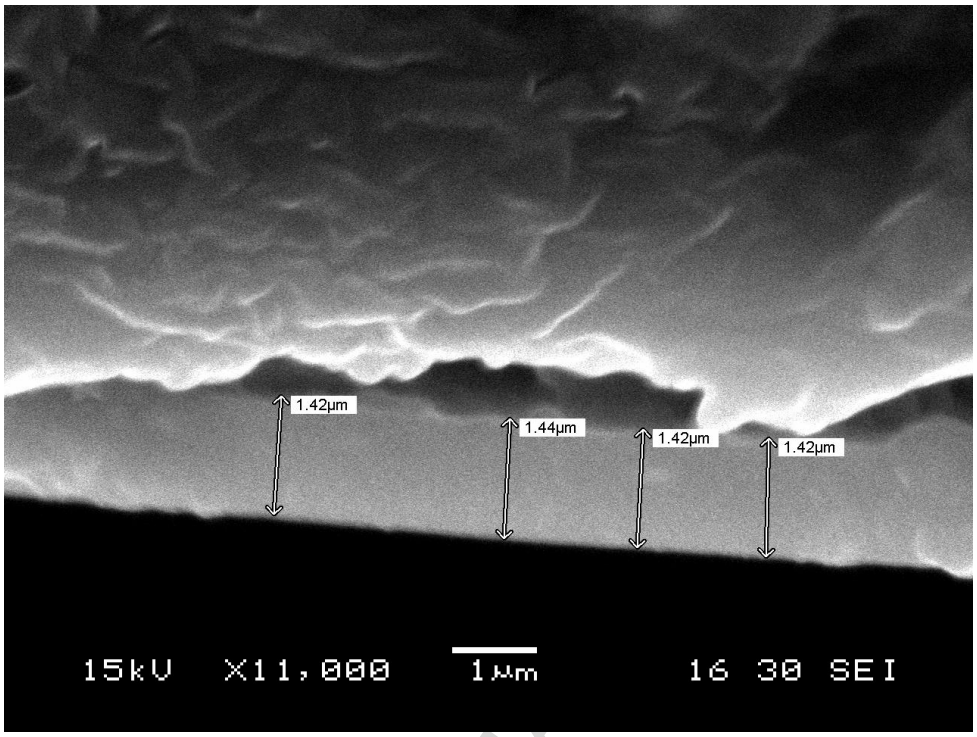

Fig. 1

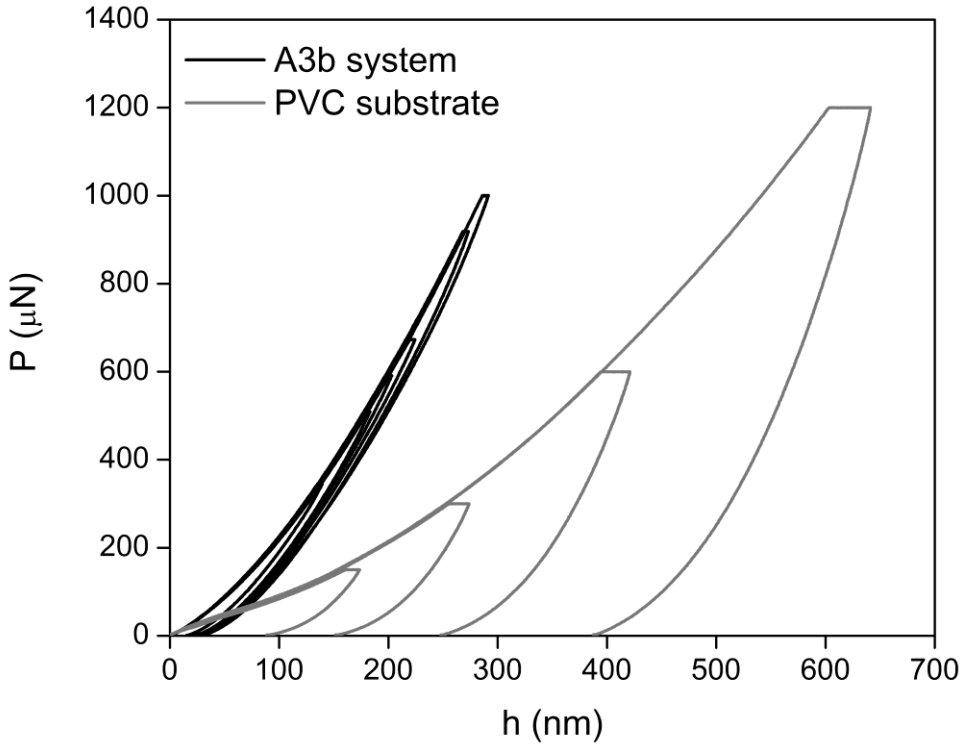

Fig. 2a

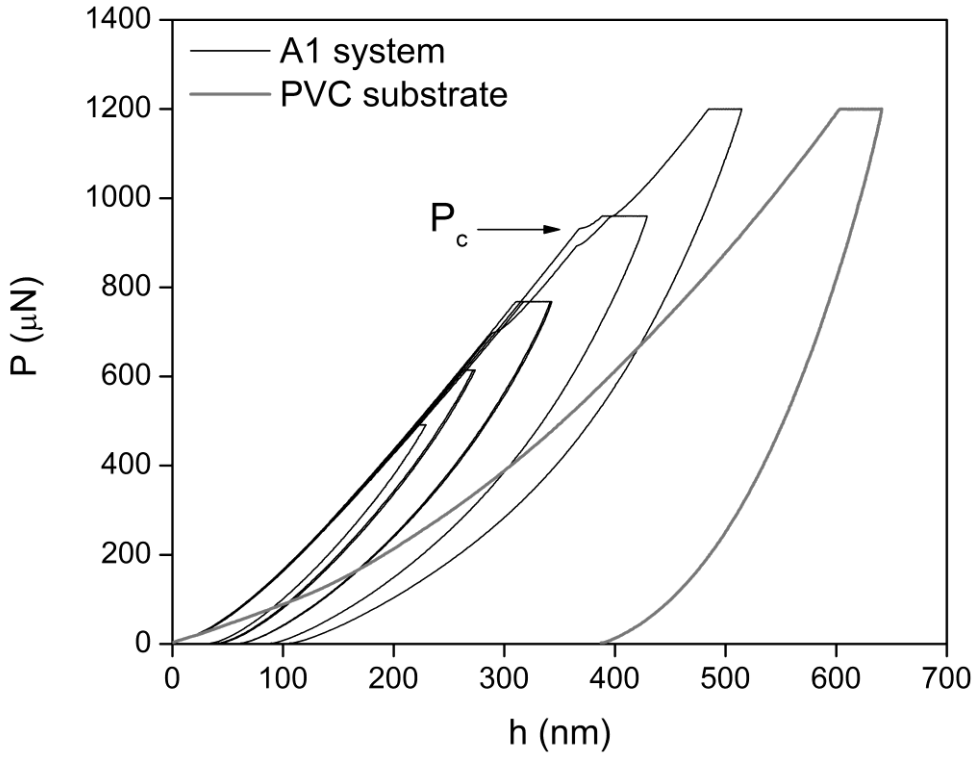

Fig. 2b

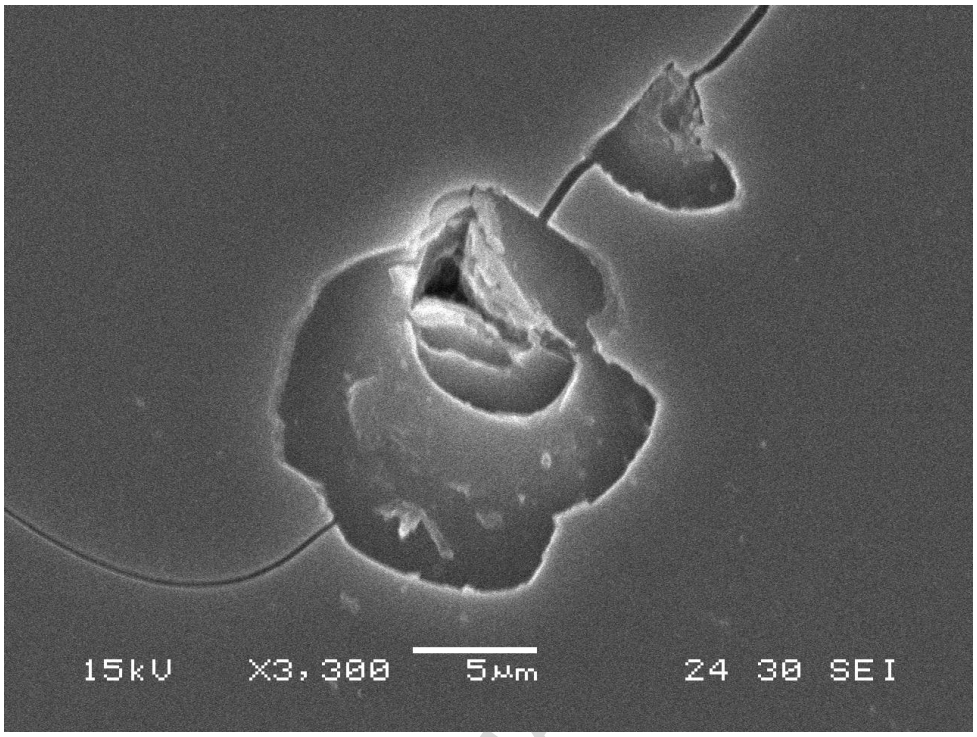

Fig. 3

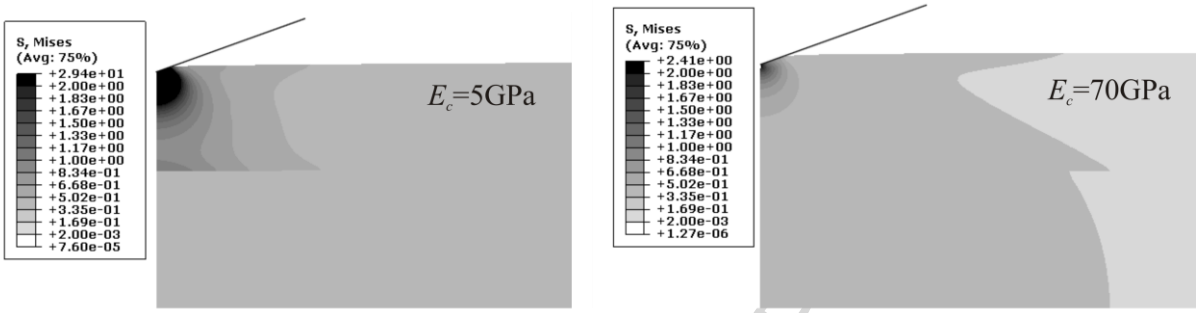

Fig. 4a

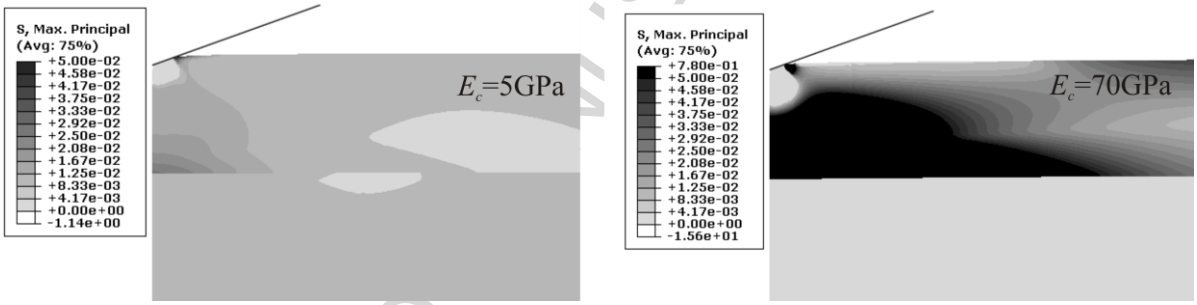

Fig. 4b

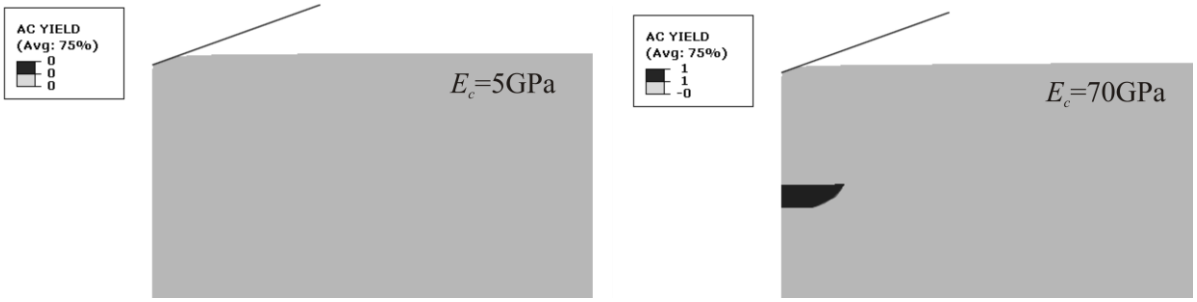

Fig. 4c

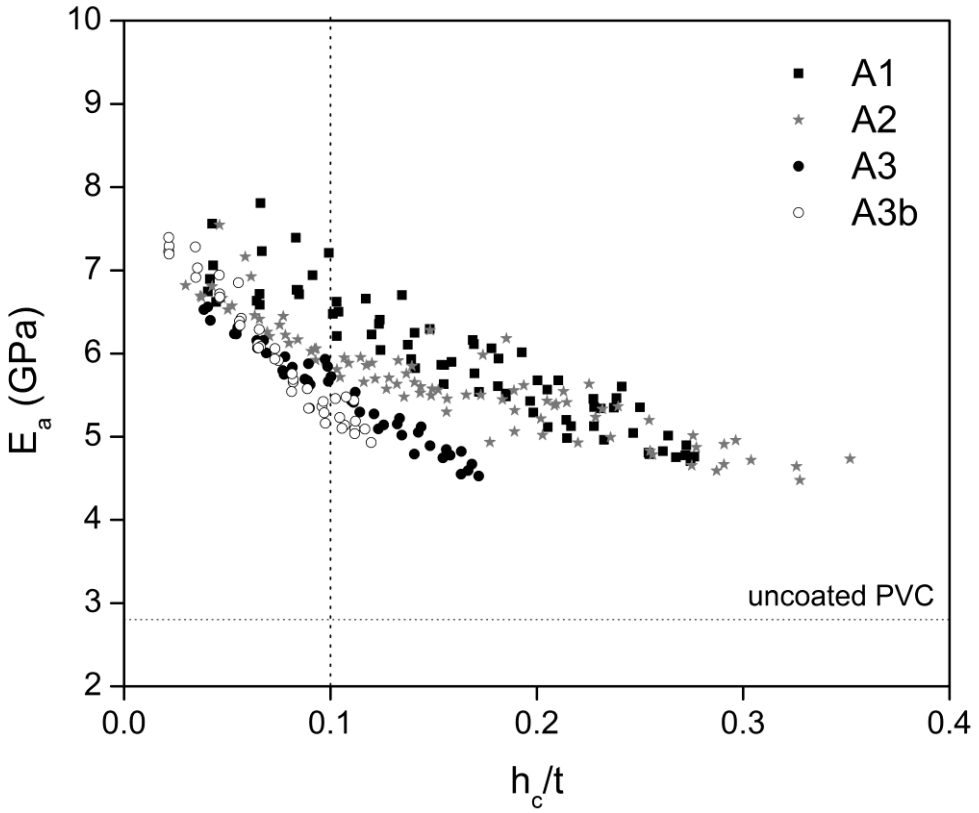

Fig. 5

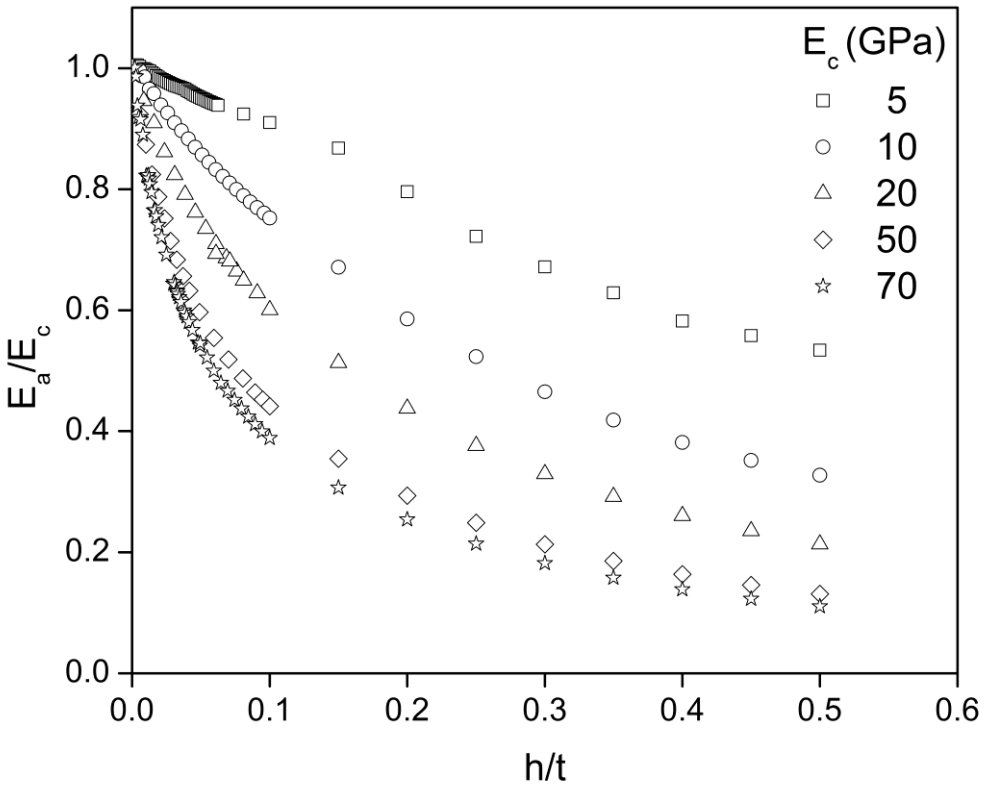

Fig. 6

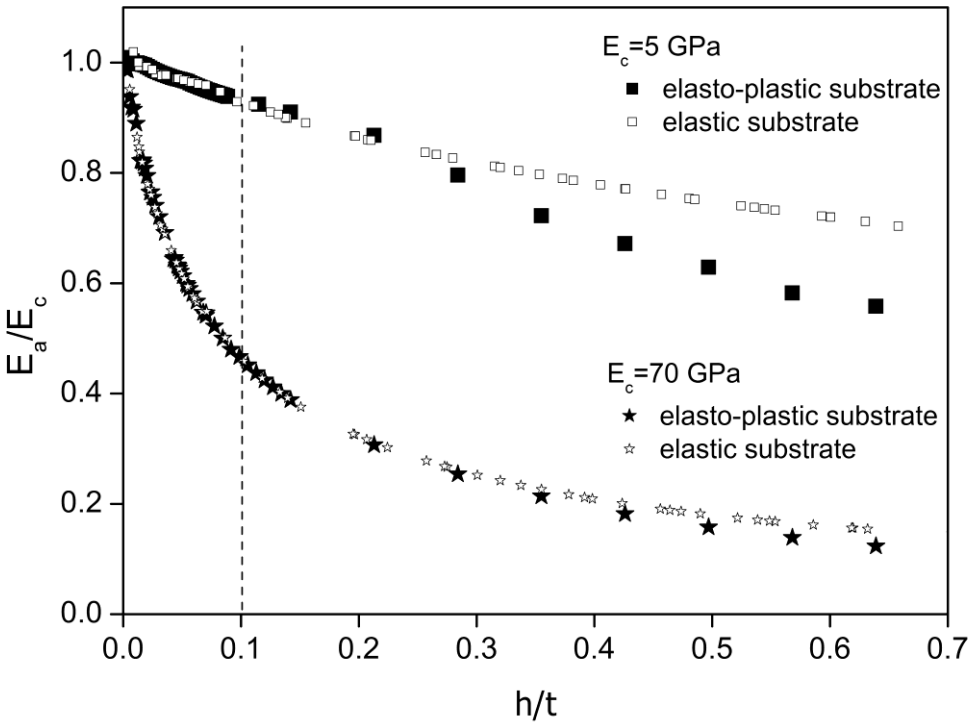

Fig. 7

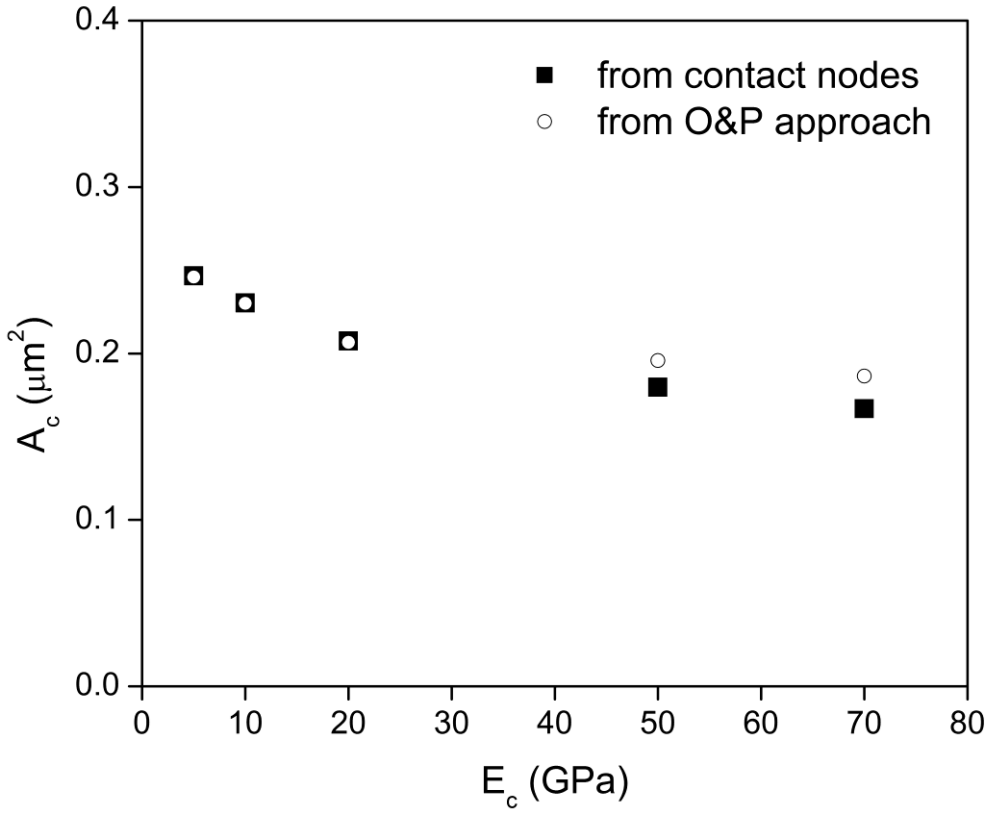

Fig. 8

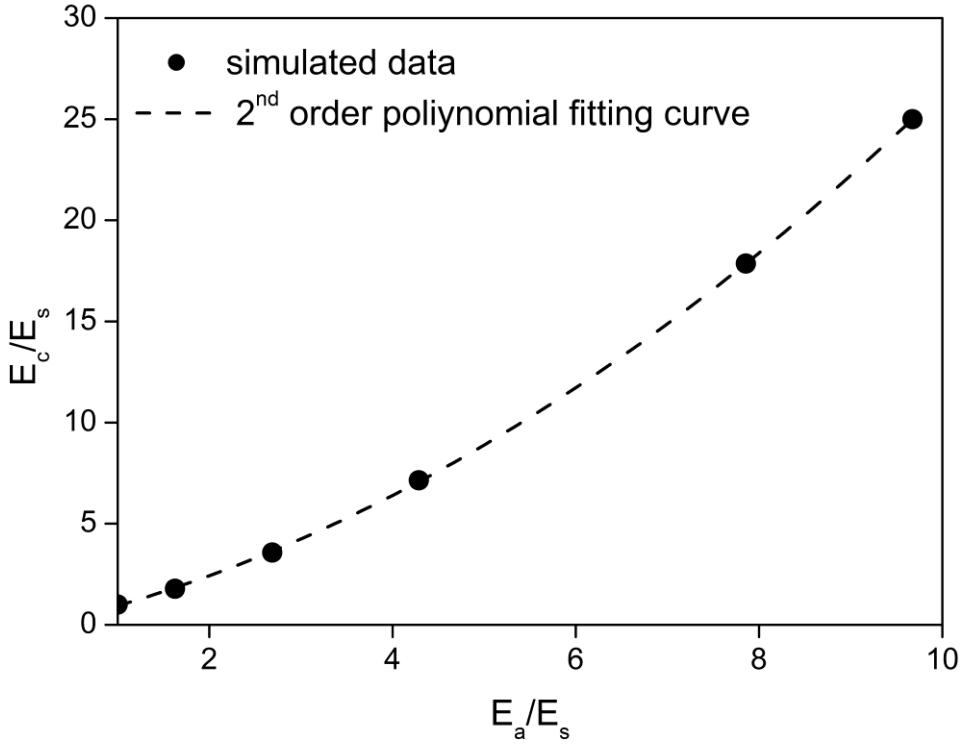

Fig. 9

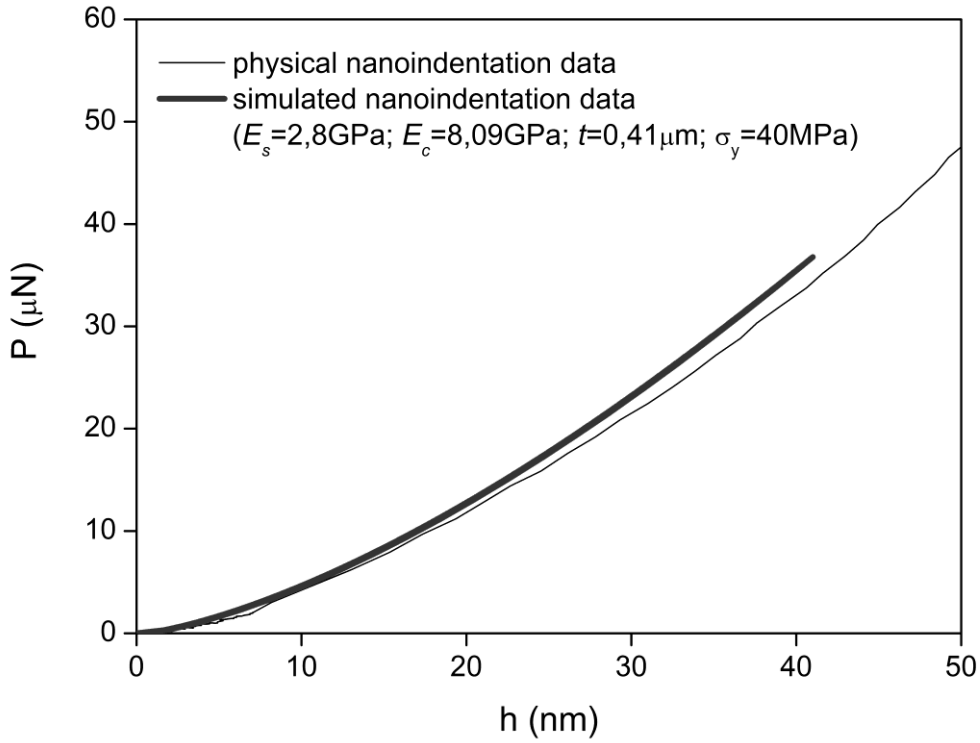

Fig. 10

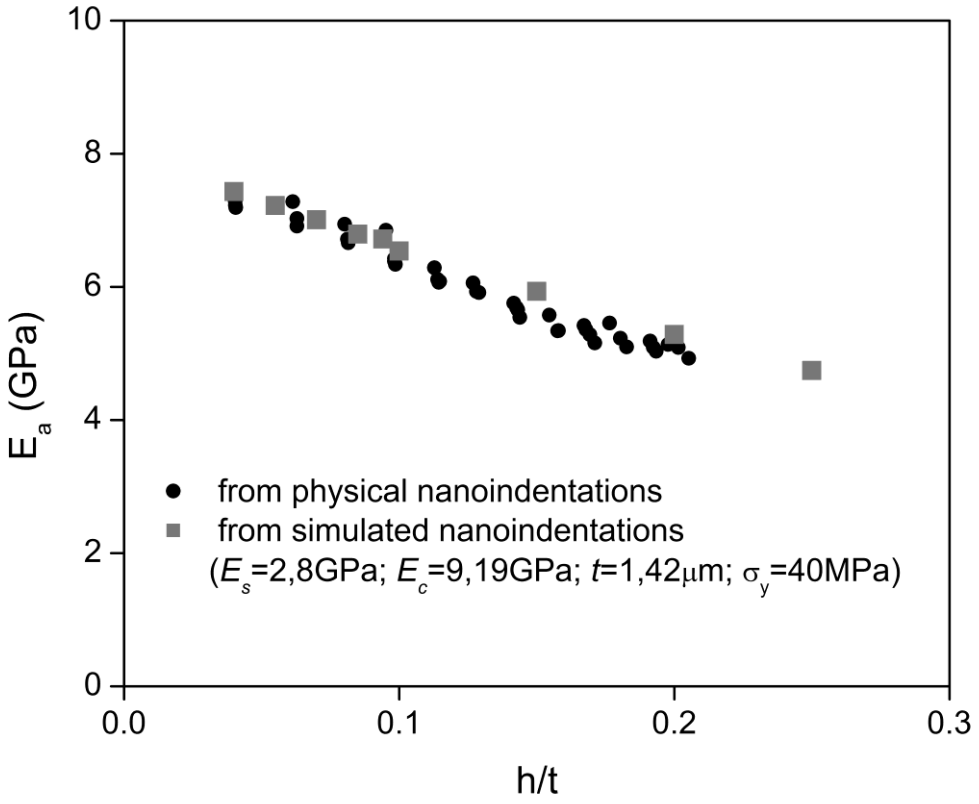

Fig. 11

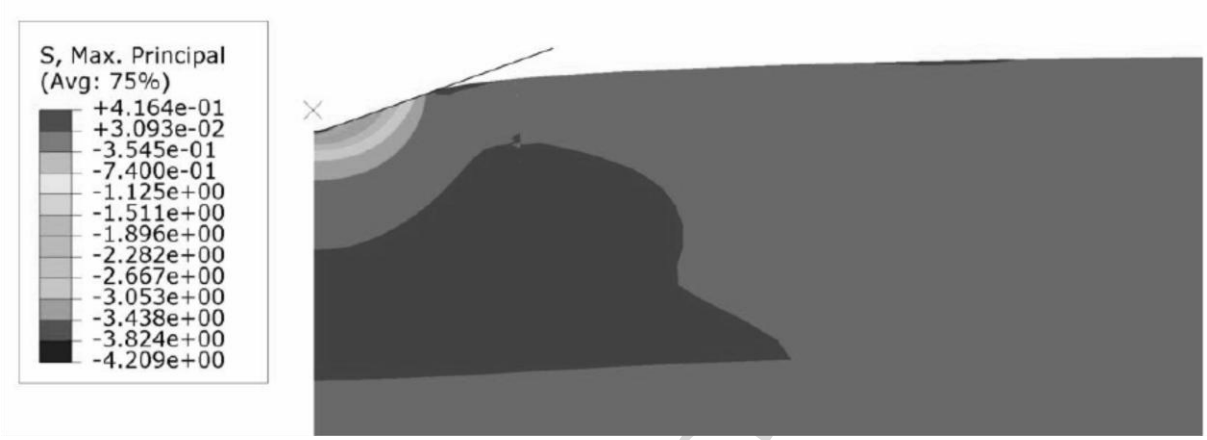

Fig. 12

HIGHLIGHTS

- Several PEO-Si/SIO_2//PVC systems were characterized by depth sensing indentation.
- System behavior was properly described as elastic//elastoplastic materials in FE simulations.
- Elastic moduli determined by Oliver-Pharr approach decreased with indentation depth.
- Intrinsic PEO-Si/SIO_2 elastic moduli were extracted from apparent values via FEA.
- A long curing time had a slight effect on hybrids moduli but weakened interfacial strength.